

Anisotropic strain-dependent material properties of bovine articular cartilage in the transitional range from tension to compression

Nadeen O. Chahine^a, Christopher C-B. Wang^b, Clark T. Hung^b, Gerard A. Ateshian^{a,*}

^a *Musculoskeletal Biomechanics Laboratory, Department of Biomedical Engineering, Columbia University, New York, NY 10027, USA*

^b *Cellular Engineering Laboratory, Department of Biomedical Engineering, Columbia University, New York, NY 10027, USA*

Accepted 1 December 2003

Abstract

Articular cartilage exhibits complex mechanical properties such as anisotropy, inhomogeneity and tension–compression nonlinearity. This study proposes and demonstrates that the application of compressive loading in the presence of osmotic swelling can be used to acquire a spectrum of incremental cartilage moduli (E_{Yi}) and Poisson's ratios (ν_{ij}) from tension to compression. Furthermore, the anisotropy of the tissue can be characterized in both tension and compression by conducting these experiments along three mutually perpendicular loading directions: parallel to split-line (1-direction), perpendicular to split-line (2-direction) and along the depth direction (3-direction, perpendicular to articular surface), accounting for tissue inhomogeneity between the surface and deep layers in the latter direction. Tensile moduli were found to be strain-dependent while compressive moduli were nearly constant. The peak tensile (+) Young's moduli in 0.15 M NaCl were $E_{+Y1} = 3.1 \pm 2.3$, $E_{+Y2} = 1.3 \pm 0.3$, $E_{+Y3}^{\text{Surface}} = 0.65 \pm 0.29$ and $E_{+Y3}^{\text{Deep}} = 2.1 \pm 1.2$ MPa. The corresponding compressive (–) Young's moduli were $E_{-Y1} = 0.23 \pm 0.07$, $E_{-Y2} = 0.22 \pm 0.07$, $E_{-Y3}^{\text{Surface}} = 0.18 \pm 0.07$ and $E_{-Y3}^{\text{Deep}} = 0.35 \pm 0.11$ MPa. Peak tensile Poisson's ratios were $\nu_{+12} = 0.22 \pm 0.06$, $\nu_{+21} = 0.13 \pm 0.07$, $\nu_{+31}^{\text{Surface}} = 0.10 \pm 0.03$ and $\nu_{+31}^{\text{Deep}} = 0.20 \pm 0.05$ while compressive Poisson's ratios were $\nu_{-12} = 0.027 \pm 0.012$, $\nu_{-21} = 0.017 \pm 0.007$, $\nu_{-31}^{\text{Surface}} = 0.034 \pm 0.009$ and $\nu_{-31}^{\text{Deep}} = 0.065 \pm 0.024$. Similar measurements were also performed at 0.015 M and 2 M NaCl, showing strong variations with ionic strength. Results indicate that (a) a smooth transition occurs in the stress–strain and modulus–strain responses between the tensile and compressive regimes, and (b) cartilage exhibits orthotropic symmetry within the framework of tension–compression nonlinearity. The strain-softening behavior of cartilage (the initial decrease in E_{Yi} with increasing compressive strain) can be interpreted in the context of osmotic swelling and tension–compression nonlinearity.

© 2004 Elsevier Ltd. All rights reserved.

Keywords: Strain-softening; Tension–compression nonlinearity; Osmotic swelling pressure; Anisotropy

1. Introduction

Articular cartilage is a multiphasic material composed of a solid phase, containing chondrocytes, proteoglycans (PG) and type II collagen, a fluid phase of water and a mobile ionic phase (Maroudas, 1979; Mow and Ratcliffe, 1997). The presence of negatively charged PGs attracts water molecules into the tissue causing it to swell when equilibrated in a physiological solution containing dissolved electrolytes. The imbalance of ions between the interstitial and extra-tissue volumes gives

rise to an osmotic pressure that is balanced by tension in the collagen fibrils (Fry and Robertson, 1967; Setton et al., 1998). This swelling pressure, reported to vary from 0.02 to 0.2 MPa (Maroudas, 1979; Basser et al., 1998; Narmoneva et al., 1999), induces a tensile state of stress, known as prestress (Fry and Robertson, 1967; Setton et al., 1998). The small associated swelling strains (Maroudas and Venn, 1977; Setton et al., 1998) are consistent with the high tensile stiffness of the solid matrix (Kempson et al., 1973; Woo et al., 1976). Indeed the tensile properties of cartilage have been measured using osmotic swelling experiments, when the free-swelling equilibrium state is taken to be the reference configuration for subsequent deformations (Basser et al., 1998; Narmoneva et al., 1999).

Articular cartilage behaves differently when loaded in tension and compression, a phenomenon known as

*Corresponding author. Department of Mechanical Engineering, Columbia University, SW Mudd, 500 West 120th Street, Mail Code 4703 New York, NY 10027, USA. Tel.: +1-212-854-8602; fax: +1-212-854-3304.

E-mail address: ateshian@columbia.edu (G.A. Ateshian).

tension–compression nonlinearity. For decades, it has been documented that articular cartilage behaves nonlinearly and possesses a higher stiffness in tension (Kempson et al., 1968; Roth and Mow, 1980; Akizuki et al., 1986), while its compressive stiffness is smaller and stress–strain response is generally linear (Mow et al., 1980; Armstrong and Mow, 1982). Furthermore, studies have shown that Poisson's ratio under uniaxial tension, generally between 0.5 and 2 (Woo et al., 1979; Elliott et al., 2002), can be considerably larger than the equilibrium compressive Poisson's ratio which ranges from 0.02 to 0.4 (Jurvelin et al., 1997; Wong et al., 2000; Wang et al., 2002, 2003). To date, this disparity between the tensile and compressive behavior has mostly been identified in separate experiments testing the tensile or the compressive properties on samples of different geometries and on tissue obtained from different areas of the joint surface. Recent experimental studies have confirmed the presence of tension–compression nonlinearity in adjacent samples of cartilage (Huang et al., 1999), and in tissue loaded perpendicular to the articular surface (Laasanen et al., 2003).

Articular cartilage is an inhomogeneous tissue whose varying biochemical composition and structure with depth (Maroudas, 1979; Mow and Ratcliffe, 1997) result in depth-dependent mechanical properties (Kempson et al., 1968; Akizuki et al., 1986; Schinagl et al., 1997; Wang et al., 2002, 2003). Cartilage has also been shown to be anisotropic in tension, with the tensile stiffness exhibiting a higher value parallel to the split line direction, the preferred orientation of collagen fibrils in the superficial zone, than perpendicular to it (Kempson et al., 1968; Akizuki et al., 1986). Furthermore, our recent studies have demonstrated that cartilage exhibits material properties consistent with orthotropic symmetry when taking into account its tension–compression nonlinearity and inhomogeneity (Wang et al., 2003), with the planes of symmetry defined locally by the direction parallel to the local split lines (1-direction), perpendicular to the split lines (2-direction), and normal to the articular surface (3-direction).

The existence of complex mechanical properties such as tension–compression nonlinearity, anisotropy and inhomogeneity, bestow a specialized load-bearing capacity on articular cartilage. The higher stiffness in tension versus compression allows cartilage to resist radial expansion under axial compressive loading and results in increased fluid pressurization and dynamic stiffness (Cohen et al., 1998; Soulhat et al., 1999; Fortin et al., 2000; Soltz and Ateshian, 2000; Huang et al., 2001).

Strain-softening of articular cartilage, a decrease in stiffness with increasing compressive strain, has been observed in a few studies at small strains (Schinagl et al., 1997; Bursac et al., 1999; Wang et al., 2003). Microstructural models have physically interpreted this phenomenon as a release of tension and buckling of

collagen fibers during compression, as the applied compressive stress overcomes the osmotic swelling pressure (Lanir, 1987; Schwartz et al., 1994; Bursac et al., 2000).

In the current study, we confirm from theory that the strain-softening effect can be interpreted in the context of tension–compression nonlinearity and osmotic swelling. We propose that the application of compressive loading in the presence of osmotic swelling can be used to acquire a spectrum of cartilage moduli from tension to compression, with the peak tensile strain achieved under hypotonic free swelling. Furthermore, the anisotropy of the tissue is characterized in both tension and compression by conducting these experiments along various loading directions. An examination of the stress–strain response over a range of tensile to compressive strains will provide evidence to whether an abrupt change in slope exists in the transition from tension to compression. Since tissue swelling and the strain-softening behavior occur over a small range of strains, we employ a microscopic technique with optimized digital image correlation (Wang et al., 2002) to examine the transition from tension to compression in the response to osmotic and compressive loading of articular cartilage.

2. Materials and experimental methods

2.1. Specimen preparation

Full-thickness osteochondral plugs (\varnothing 4 mm) were harvested from the humeral head of five healthy 3–4 month-old immature bovine glenohumeral joints. Following harvest, the plugs were rinsed with a solution of phosphate-buffered saline (PBS) and protease inhibitors (PI, Complete protease inhibitor cocktail tablets, Roche Applied Science, IN) and stored at -80°C . On the day of testing, each plug was immersed in freshly prepared PBS + PI and all subchondral bone and blood vessels were removed using a sledge microtome (Model 1400; Leitz, Rockleigh, NJ, USA) equipped with a freezing stage (Hacker Instruments, Fairfield, NJ, USA). Next, the articular surface was lightly punctured with a round-tip needle and examined under a 10X lens (Olympus America, Melville, NY, USA) of a microscope in order to determine the split-line direction (1-direction). The split-line direction was marked with a parallel cut on the periphery of the cartilage plug (Fig. 1a). A cubic specimen ($0.9\text{ mm} \times 0.9\text{ mm} \times \text{thickness}$) was sharply excised relative to the split-line direction using a custom cutting device equipped with orthogonal blades (Fig. 1b). One face of the cube, defined by the split-line direction (1-direction) and the depth direction (3-direction), was marked using Trypan Blue dye (0.4% in PBS; Sigma, St. Louis, MO, USA). During

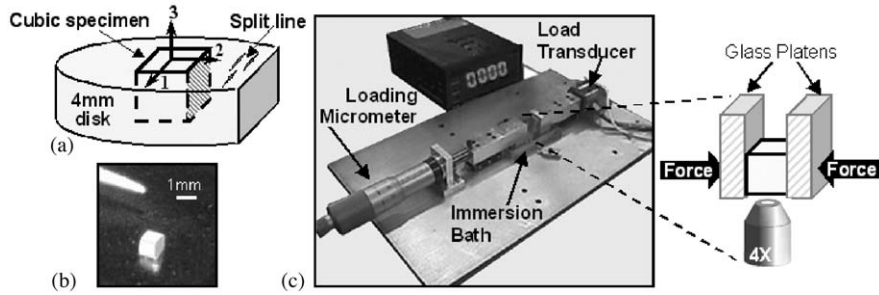


Fig. 1. (a) Specimen preparation relative to the split line direction; (b) cubic sample of cartilage; (c) uniaxial unconfined compression loading device. Cubic samples are loaded between two glass platens while visualized using an inverted microscope.

all subsequent testing, specimen orientation was determined using this marked face and the easily discernible articular surface. The dimensions of each specimen were optically measured using a calibrated 4X objective (UPlan 4X; Olympus) with a resolution of $1.66 \mu\text{m}/\text{pixel}$. The remainder of the cartilage plug was stored at -20°C for biochemical analysis to determine the water content and fixed charge density of the tissue.

2.2. Loading protocol

The cubic specimens were loaded in unconfined compression using a custom loading device (Fig. 1c) and a previously described protocol (Wang et al., 2002, 2003). Briefly, uniaxial compressive deformation was manually applied using a micrometer with $1 \mu\text{m}$ resolution (MRO Industrial Supplies, Manville, NJ, USA), and the resultant compressive equilibrium load was recorded using a load transducer (Model 31; Sensotec Inc, Columbus, OH, USA, 0–50 g). The sample was positioned between two parallel glass-loading platens (Fig. 1c) and was surrounded by NaCl + PI solution in an immersion chamber. The device was positioned on a motorized stage (ProScan H128 Series; Prior Scientific, Rockland, MA, USA) of an inverted microscope (Olympus IX70; Olympus) and aligned so that the platens were perpendicular to the moving axis of the stage. The optical path of the microscope was adjusted through the immersion chamber, and the face of the cubic specimen between the platens was visualized. Images were acquired using a digital camera (MicroMax 5 MHz; Princeton Instruments, Trenton, NJ USA) and stored for further analysis (Wang et al., 2002).

Twenty-four cubic specimens were equally divided into three groups, with group i specifically used to study the bathing concentration effects on loading in the i -direction ($i=1-3$). For each specimen, the loading response was measured in the presence of three external bathing solutions (0.015, 0.15 and 2 M NaCl), tested in random order with 0.15 M considered the physiological ionic level. In each trial, the specimen was equilibrated in a bathing solution for 40 min and an image was acquired at its free-swelling state. Compression was then

applied in 2% increments relative to the uncompressed tissue thickness, h_0 , along the desired loading direction. After each compressive increment the specimen was allowed to relax for 20 min, a period sufficient for equilibrium to be attained in these small samples, as was determined in our previous study (Wang et al., 2003). At equilibrium, an image of the entire visible face of the cubic sample was acquired and the resultant load was recorded. Deformation was incrementally applied until strain reached 20% of h_0 , at which point the specimen was allowed to recover for 40 min, the bathing solution was changed to another concentration and the loading protocol repeated. Despite the ~ 13 h duration of a typical test, biochemical measurements conducted in our laboratory as part of other studies, on similar tissue, have shown no significant loss of proteoglycan or collagen content for incubation periods up to 18 h in PBS.

Strain analyses were performed across the entire imaged face using an optimized digital image correlation (DIC) technique as previously described (Wang et al., 2002). Accurate axial (E_{ii}^a) and lateral (E_{jj}^a) strains were calculated from the tissue images, relative to the free-swelling configuration, by automatically tracking and quantifying the displacement fields within the tissue. (The superscript a in E_{ij}^a denotes “applied” strain, which is the strain relative to the free-swelling configuration, see the Appendix.) The equilibrium normal stress (σ_{ii}) was calculated from the measured load and cross-sectional area; the effective incremental Young’s modulus (E_{Yi}^{eff}) along the i -direction and Poisson’s ratio (ν_{ij}) for loading in the i -direction and expansion in the j -direction were evaluated from the slope of σ_{ii} versus E_{ii}^a and the slope of E_{jj}^a versus E_{ii}^a , respectively:

$$E_{Yi}^{\text{eff}} = \frac{\partial \sigma_{ii}}{\partial E_{ii}^a}, \quad \nu_{ij} = -\frac{\partial E_{jj}^a}{\partial E_{ii}^a} \quad (1)$$

2.3. Biochemical analyses

Each remainder of the cartilage plug was thawed at room temperature; excess fluid was blotted, and tissue was transferred to pre-weighed vials. The vials were

sealed to minimize dehydration and the wet weight of the tissue was measured using an analytical balance. The samples were then lyophilized in a vacuum desiccator for 48 h and reweighed to determine the dry weight. The porosity, or water content, was calculated as the percentage difference between wet and dry weights. Cartilage samples were then digested using papain (20 μ l per 100 mg tissue; Sigma) at 60°C overnight. The glycosaminoglycan (GAG) content was measured using the 1,9 dimethylmethylene blue assay (Farndale et al., 1982) with chondroitin-6-sulfate (CS; Sigma) as the standard. The fixed charge density (c_0^F) was calculated as $c_0^F = z_{CS}c_{GAG}/M_{CS}$; where c_{GAG} is mg of GAG per ml of water, and M_{CS} and z_{CS} are the molecular weight and number of charges per CS disaccharide, respectively ($z_{CS} = 2$ charges/repeating unit; $M_{CS} = 513$ g/repeating unit) (Narmoneva et al., 1999).

2.4. Statistical analyses

Statistical analysis was performed on all experimental results using two-way ANOVA for strain and bathing concentration dependence, and a repeated measure analysis was also used when testing the differences between the surface and deep layers of loading in 3-direction. Tukey HSD post hoc test was applied with $p < 0.05$ considered statistically significant.

3. Results

Axial compression of articular cartilage in the 1- and 2-directions produced linear displacement fields along the 2- and 1-directions, respectively, and thus uniform strain fields across the entire imaged face. Loading along the 3-direction resulted in nonlinear displacements from the superficial to the deep zone as previously reported (Guilak et al., 1995; Schinagl et al., 1997; Wang et al., 2002, 2003), yielding inhomogeneous strain fields in the axial direction; however the lateral strain field (normal strain along the 1-direction) remained uniform throughout the thickness. The homogenous strain components, E_{11}^a and E_{22}^a , were calculated using linear regression of the displacement fields. The inhomogeneous strain E_{33}^a was approximated with a bilinear response, such that the cartilage exhibits distinct strains in the top $\frac{1}{3}$ and the bottom $\frac{2}{3}$ of the tissue thickness, consistently with our earlier study (see Fig. 4 in Wang et al., 2003); therefore distinct values of E_{Y3} and v_{31} are reported for each layer. Under physiological bathing conditions, the tissue deformed by $42.6 \pm 5.4\%$ and $11.4 \pm 1.7\%$ in the surface and deep layers, respectively, when a 20% platen-to-platen deformation was applied. In this study, we present the results along the 3-direction for the deep layer up to the point of maximum measured strain, and

the results of the surface layer are limited to the range of small strain (i.e. $\leq 20\%$).

The average stress–strain response over all specimens, for each of the three loading directions, is presented in Fig. 2. The specimens initially demonstrated a nonlinear stress–strain response, transitioning to a linear response with increasing strain. The incremental Young's moduli along the three directions (E_{Yi}), determined from the slope of the stress–strain responses (using a backward first-order finite difference scheme), are presented in Fig. 3. These moduli also exhibited nonlinearity near the free-swelling reference state, decreasing progressively with applied strain until reaching a constant value. We refer to the decrease in modulus with increasing compression relative to the reference free-swelling state as strain-softening. Stress magnitudes (Fig. 2) and Young's moduli (Fig. 3) were highest under hypotonic conditions (0.015 M NaCl), and decreased significantly under isotonic (0.15 M; $p < 0.001$) and hypertonic (2 M; $p < 0.001$) conditions.

The incremental Poisson's ratios, shown in Fig. 4, displayed a similar strain-dependent behavior along all loading directions and at all bathing concentrations. The average Poisson's ratio was greatest at the free-swelling

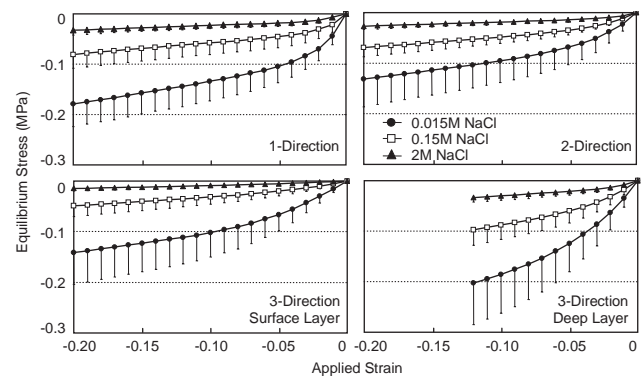


Fig. 2. Resultant stress measured for loading in 1-direction ($n = 8$), 2-direction ($n = 8$) and surface and deep layers of 3-direction ($n = 8$) in presence of three bathing concentrations.

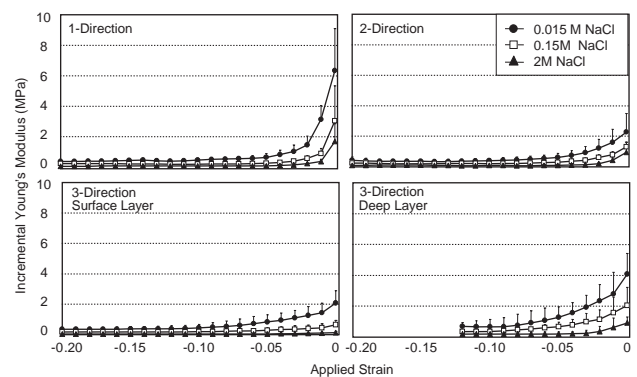


Fig. 3. Strain-dependent incremental Young's modulus measured for loading in 1-direction ($n = 8$), 2-direction ($n = 8$), and both surface and deep layers of 3-direction ($n = 8$).

reference state and decreased nonlinearly to a near constant value with increasing compression. Poisson ratios were also highest under hypotonic conditions,

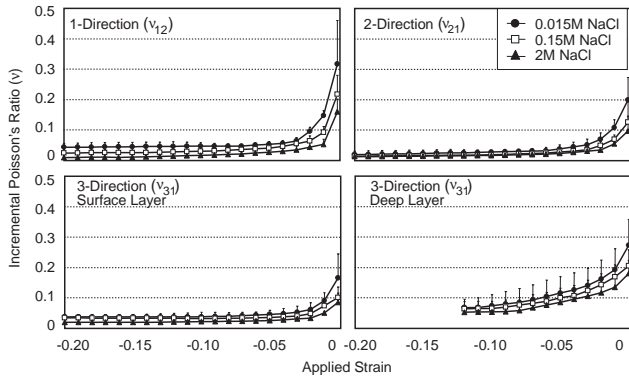


Fig. 4. Incremental Poisson's ratios for all loading groups: 1-direction ($n=8$), 2-direction ($n=8$), surface and deep layers of 3-direction ($n=8$), in the presence of three bathing solutions.

decreasing significantly with increasing salt concentration ($p < 0.001$).

The values of E_{Yi} at the free-swelling reference state and at the highest applied compressive strain are shown in Fig. 5a and b, respectively (note the different scales). For reasons further discussed below, the values at the free-swelling reference state (i.e., zero applied strain) are described as peak tensile moduli (E_{+Yi}) whereas the values at the highest applied strain are described as compressive moduli (E_{-Yi}). The corresponding tensile and compressive values of incremental Poisson's ratios are presented in Fig. 6a (v_{+ij}) and b (v_{-ij}), respectively (note the different scales). Statistical differences among the various loading directions are specified on these figures.

The free-swelling normal strain along the i th direction, E_{ii}^0 , which represents the tensile strain in the solid matrix in the free-swelling reference state, was determined relative to the point where the solid matrix strain is zero (see the Appendix). It was assumed that the solid

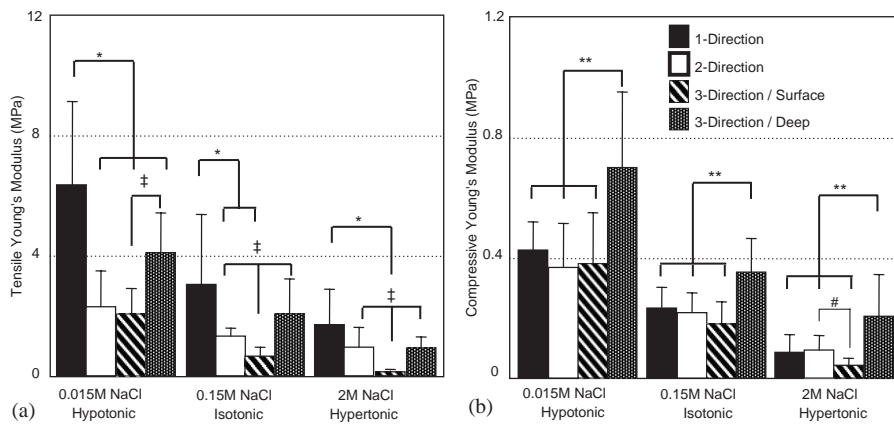


Fig. 5. Summary of the (a) tensile and (b) compressive Young's moduli for all loading groups and bathing concentrations. Note the different scales along the ordinate. The tensile and compressive moduli were derived from the slope of the stress–strain curve at the point of zero strain and the highest applied strain, respectively. ($*p < 0.03$ between 1-direction and other groups as shown; $‡p < 0.02$ between surface layer of 3-direction and other groups as shown; $**p < 0.001$ between deep layer of 3-direction and other groups as shown; $\#p < 0.0002$ between surface and deep layer of 3-direction).

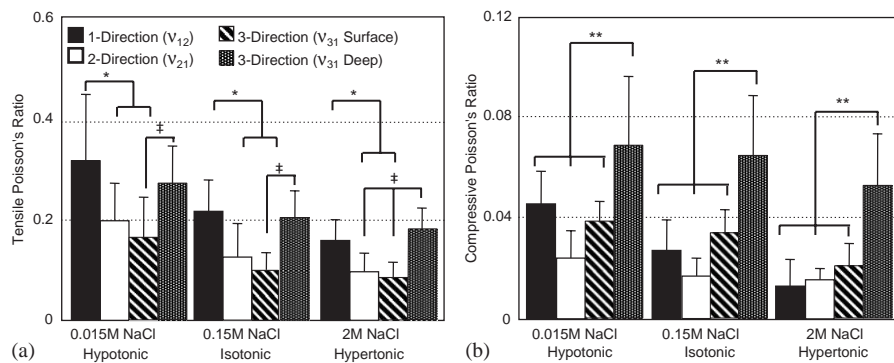


Fig. 6. Summary of (a) tensile and (b) compressive Poisson's ratios under all loading conditions and ionic environments. Note the different scales along the ordinate. The tensile and compressive Poisson's ratios correspond to the points of zero strain and highest applied strain of the stress–strain response, respectively. ($*p < 0.03$ in 1-direction versus 2-direction and surface layer of 3-direction; $‡p < 0.02$ between surface and deep layers of 3-direction; $**p < 0.05$ relative to deep layer of 3-direction).

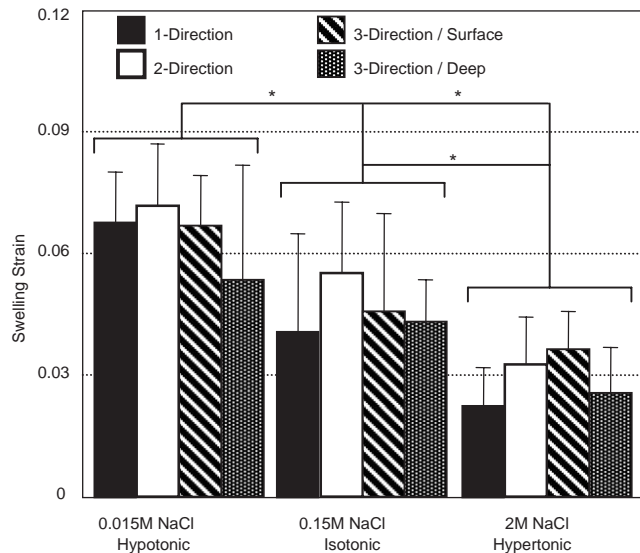


Fig. 7. Swelling strain measured in the three loading directions and in the presence of hypotonic, physiological and hypertonic bathing solutions. The swelling decreased with increasing bathing concentration (* $p < 0.01$) and a nonzero swelling was measured in hypertonic conditions ($p < 0.0001$).

matrix strain is zero at the transition point between the linear stress–strain regime and the nonlinear stress–strain regime (Fig. 2). Because of the uncertainty inherent in the determination of this point in the presence of noisy data, E_{ii}^0 was calculated as the point at which the stress–strain response deviated outside of the 95% confidence interval determined from the regression analysis of the linear region (Fig. 7). The free-swelling strain under hypotonic conditions was significantly greater than under isotonic ($p < 0.001$) and hypertonic ($p < 0.0001$) conditions.

The average porosities, or water content, were determined to be 0.852 ± 0.028 , 0.849 ± 0.012 and 0.859 ± 0.022 for the three loading groups, respectively, with no significant differences among the groups ($p > 0.5$). Similarly no significant differences were found in fixed charge densities among the three groups (0.132 ± 0.024 mEq/ml for samples loaded in 1-direction, 0.121 ± 0.019 mEq/ml for 2-direction and 0.121 ± 0.030 mEq/ml for 3-direction; $p > 0.4$).

4. Discussion

The objective of this study was to acquire a spectrum of cartilage moduli from tension to compression using compressive loading in the presence of osmotic swelling, and to investigate whether or not an abrupt change in slope exists in the transition from tension to compression. Based on previous findings that the tissue is orthotropic, these measurements were performed along

the three previously identified directions of material symmetry.

A major finding of the current study is that the strain-softening behavior of cartilage is much more significant than previously observed (Schinagl et al., 1997; Bursac et al., 1999; Wang et al., 2003), when sufficiently small compressive strain increments are applied (Figs. 2 and 3). The application of microscopy techniques has allowed for the examination of small strain levels ($< 5\%$) in cartilage, without having to rely on the measurement of distance between loading platens, because strain is determined from the texture on the face of the sample before and after load application. In contrast, in most traditional compressive studies of cartilage, including our own, the strain-softening behavior was not typically observed, possibly because the application of a tare load (a common experimental procedure for setting the initial state of contact between the tissue and loading platens) would produce a compressive strain that typically surpasses the range of strains over which softening occurs ($\sim 0\%$ to 5% at 0.15 M NaCl, Fig. 7). Beyond the small strain response (e.g., $> 20\%$), it is well established that cartilage exhibits nonlinear strain-stiffening (Kwan et al., 1990; Ateshian et al., 1997; Schinagl et al., 1997).

The effective uniaxial unconfined modulus of the tissue, varies over a wide range, decreasing for example from 3.1 ± 2.3 MPa at the free-swelling state to 0.23 ± 0.07 MPa at 20% compression under isotonic conditions (0.15 M NaCl), parallel to the split-line direction (Fig. 5). This disparity is consistent with literature measurements of equilibrium tensile properties (Roth and Mow, 1980; Myers et al., 1984; Schmidt et al., 1990) versus compressive properties (Wang et al., 2003) of bovine articular cartilage along that direction. Furthermore, this observation supports the hypothesis that the strain-softening is a manifestation of osmotic swelling, which places the collagen–proteoglycan matrix under an initial state of tensile strain (Fig. 8) in the presence of an osmotic load. When the applied compressive strain is smaller than the swelling strain, the solid matrix remains in a state of tension and the slope of the stress–strain response represents the tensile modulus. Conversely, when loading is initiated from a reference compressive strain that exceeds the free-swelling strain, the stress–strain response occurs entirely over the compressive range and the slope represents the compressive modulus (Fig. 8).

The strain-softening behavior observed in this study is an inescapable consequence of matrix tension–compression nonlinearity in the presence of osmotic swelling, as indicated from a straightforward theoretical analysis (Appendix, Fig. 8). Since the osmotic pressure of proteoglycans and tension–compression nonlinearity of the solid matrix of cartilage are well established, this study does not offer a new paradigm for cartilage

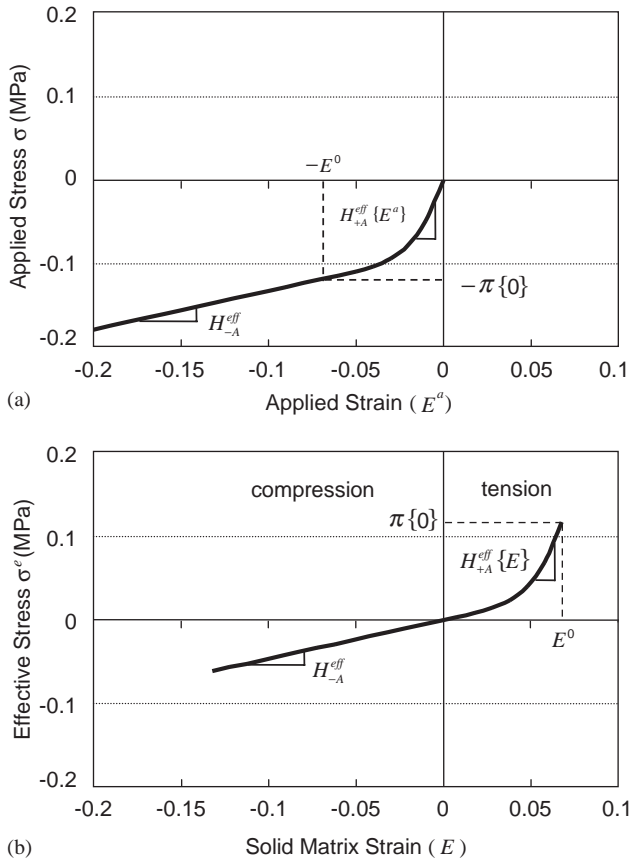


Fig. 8. (a) Plot of $\sigma\{E^a\}$ versus E^a based on Eq. (A.10). (b) Plot of $\sigma\{E\} + \pi\{0\} \approx \sigma^e\{E\}$ versus E based on Eq. (A.9). Representative values of the material constants are taken from Table 1 for 0.015 M NaCl, along the 1-direction.

mechanics but simply provides experimental data in support of a predictable mechanism. In contrast to the observation that E_{-Y1} remains nearly constant, E_{+Y1} is strongly strain dependent over the range of strains measured in this study. It is clearly evident from Figs. 2 and 3 that the transition from tension to compression occurs smoothly, with no observable jump in the modulus.

Further supporting this interpretation of the results is the observed variation in the stress–strain and modulus–strain responses under various bathing salt concentrations. Since a hypotonic salt solution is known to increase the osmotic pressure in articular cartilage whereas a hypertonic solution decreases it (Maroudas, 1979; Basser et al., 1998; Narmoneva et al., 1999), the reference free-swelling strain is expected to be greatest at 0.015 M, decreasing progressively at 0.15 M and 2 M. Given that the tensile modulus is strongly strain dependent, the modulus measured at the free-swelling state in the hypotonic solution is higher, while that measured at the hypertonic state is lower than in the isotonic state (Figs. 3 and 5). For example, E_{+Y1} is equal to 6.3 ± 2.7 , 3.1 ± 2.3 and 1.7 ± 1.2 MPa at 0.015, 0.15 and 2 M, respectively.

Since the fixed charge densities measured in the three groups of specimens were not statistically different, the observed differences in material properties measured among the groups resulted primarily from tissue anisotropy. The current study confirms previous literature findings (Kempson et al., 1968; Roth and Mow, 1980; Akizuki et al., 1986) that the tensile modulus parallel to the split line direction, E_{+Y1} , is significantly greater than in the perpendicular direction E_{+Y2} ($p < 0.0005$, Fig. 5). Novel findings of the current study are that $E_{+Y1} > E_{+Y3}^{\text{Surface}}$ ($p < 0.0002$), $E_{+Y1} > E_{+Y3}^{\text{Deep}}$ ($p < 0.03$), $E_{+Y2} > E_{+Y3}^{\text{Surface}}$ ($p < 0.02$), as indicated in Fig. 5a.

The compressive Young’s moduli satisfied $E_{-Y1} \approx E_{-Y2} \approx E_{-Y3}^{\text{Deep}} < E_{-Y3}^{\text{Surface}}$ under hypotonic ($p < 0.003$) and isotonic conditions ($p < 0.0004$). In hypertonic conditions, this relationship was also observed ($p < 0.01$) along with $E_{-Y3}^{\text{Surface}} < E_{-Y2}$ ($p < 0.002$). These results are consistent with our recent study of bovine cartilage anisotropy in compression (Wang et al., 2003), with the exception that E_{-Y3}^{Surface} was previously found to be slightly (but statistically) smaller than E_{-Y1} and E_{-Y2} . This distinction may be due to differing degrees of inhomogeneity of the tissues, as the ratio of surface to deep layer strains is ~ 3.8 in the current study (compared to ~ 5.2 in Wang et al., 2003, Table 2).

This study bridges the independent experimental measurements of Poisson’s ratio in tension and compression reported in the literature (Woo et al., 1979; Jurvelin et al., 1997; Wong et al., 2000; Elliott et al., 2002; Wang et al., 2002, 2003). The results of Figs. 4 and 6 indicate that tensile Poisson’s ratios measured at the free-swelling reference state are significantly greater in magnitude than compressive Poisson’s ratios. For example, at 0.15 M, $\nu_{+12} = 0.217 \pm 0.062$ whereas $\nu_{-12} = 0.027 \pm 0.012$ (Fig. 6), with a smooth transition occurring from tension to compression over a rather narrow range of strains (Fig. 4). The smaller value in compression is consistent with our recent measurements (Wang et al., 2002, 2003), including the findings that $\nu_{-12} \approx \nu_{-21} \approx \nu_{-31}^{\text{Surface}} < \nu_{-31}^{\text{Deep}}$ ($p < 0.001$). In tension, recent studies have demonstrated that ν_{+12} can range from 0.6 to 1.9 in human patellar and glenohumeral joint cartilage (Huang et al., 1999; Elliott et al., 2002), and tends to remain constant with increasing tensile strain. The trend observed in Fig. 4 indicates that Poisson’s ratio may increase above 0.3 with increasing tensile strains, though literature results suggest that it should eventually reach a constant value. Other novel findings of this study are that $\nu_{+21} \approx \nu_{+31}^{\text{Surface}} < \nu_{+12}$ at all bathing concentrations (Fig. 6a; $p < 0.03$), and that the tensile Poisson’s ratios decrease with increasing salt concentration.

In principle the true value of the free-swelling strain cannot be determined exactly from the experimental results presented in this study, since it is calculated assuming knowledge of the state when the solid matrix

strain is zero. This study assumes that the solid matrix response exhibits a strain-dependent modulus *immediately* upon undergoing tension, so that the zero-solid-matrix-strain point may be deduced as the transition from the linear to the nonlinear stress–strain regime.

Free-swelling strains exhibited the well-expected decrease in magnitude with increasing ionic concentration (Fig. 7, $p < 0.01$), due to the concomitant decrease in osmotic pressure. However, unlike the tensile modulus (Fig. 5a), they did not exhibit statistically significant anisotropy, despite the expectation that higher tensile stiffness should produce lower swelling strain along the corresponding direction. One potential explanation for this discrepancy is that the magnitude of the swelling strain depends not only on the peak tensile modulus in the free-swelling state, but also on the length of the toe region in the nonlinear stress–strain response in the tensile regime.

The swelling strain remained significantly greater than zero under hypertonic conditions. This result is consistent with the studies of Ehrlich and co-workers which show that glycosaminoglycan solutions exhibit a non-negligible osmotic pressure even under hypertonic conditions, due to the entropic contribution to osmotic pressure (Urban et al., 1979; Ehrlich et al., 1998). The theoretical analysis presented in the Appendix suggests that this osmotic pressure magnitude may average as high as 0.016 MPa under hypertonic conditions (Table 1).

It is evident from Figs. 2 and 3 that the transition from tension to compression occurs smoothly, with no

observable jump in the modulus. This smooth transition is of great interest from a modeling perspective. In our earlier studies (Soltz and Ateshian, 2000; Ateshian et al., 2003b; Wang et al., 2003) we modeled the tension–compression nonlinearity with a bilinear stress–strain response, with a jump in the modulus at the strain origin, according to the conewise linear elasticity model (Curnier et al., 1995). For a material with orthotropic symmetry, a jump in the modulus implies that there are eight distinct orthotropic elasticity tensors at the strain origin, based on which three normal strain components are positive or negative. Satisfying the positive definiteness of all eight elasticity tensors posed a significant modeling challenge, restricting the range of acceptable material constants derived from fitting experimental data (Wang et al., 2003). With a smooth transition, only one orthotropic elasticity tensor is necessary for modeling the response at the strain origin, increasing the modeling flexibility at the price of making the elasticity tensor strain dependent in the tensile regime.

In summary, this study demonstrates that the application of mechanical loading in the presence of osmotic swelling can be used effectively to extract tensile and compressive material properties from a single sample of articular cartilage, yielding a comprehensive set of strain-dependent Young's moduli and Poisson's ratios under various ionic conditions. The results indicate that the compressive modulus remains nearly constant with increasing compression (up to 20%) whereas the tensile modulus is very strongly strain dependent, with a smooth transition occurring between

Table 1

Mean and standard deviation of material constants for the constitutive model of Eq. (A.10) from curvefitting of the experimental uniaxial stress–strain data along each loading direction, along with the corresponding coefficient of determination for the nonlinear curvefit

	H_{-A}^{eff} (MPa)	$\ln(D_A^{\text{eff}})$	n	$\pi\{0\}$ (MPa)	R^2
1-Direction					
0.015 M	0.464 ± 0.086	23.37 ± 3.69	4.50 ± 1.57	0.118 ± 0.038	0.996 ± 0.0038
0.15 M	0.236 ± 0.059	20.56 ± 2.94	3.21 ± 0.94	0.043 ± 0.020	0.995 ± 0.0037
2 M	0.098 ± 0.044	19.44 ± 2.19	2.61 ± 0.46	0.015 ± 0.007	0.994 ± 0.0041
2-Direction					
0.015 M	0.373 ± 0.121	18.01 ± 3.16	2.76 ± 1.31	0.086 ± 0.045	0.998 ± 0.0007
0.15 M	0.215 ± 0.061	17.15 ± 1.11	2.38 ± 0.42	0.039 ± 0.013	0.999 ± 0.0009
2 M	0.086 ± 0.021	18.69 ± 3.67	2.82 ± 1.35	0.013 ± 0.004	0.995 ± 0.0034
3-Direction surface					
0.015 M	0.419 ± 0.175	17.73 ± 3.93	2.50 ± 1.41	0.085 ± 0.044	0.994 ± 0.0053
0.15 M	0.185 ± 0.075	17.41 ± 2.85	2.55 ± 0.74	0.021 ± 0.013	0.997 ± 0.0042
2 M	0.054 ± 0.025	17.76 ± 2.87	2.75 ± 0.46	0.005 ± 0.003	0.995 ± 0.0051
3-Direction deep					
0.015 M	1.180 ± 0.629	17.50 ± 1.19	2.11 ± 0.32	0.130 ± 0.070	0.997 ± 0.0026
0.15 M	0.583 ± 0.209	16.76 ± 1.12	2.12 ± 0.30	0.056 ± 0.027	0.995 ± 0.0031
2 M	0.187 ± 0.072	16.95 ± 0.84	2.06 ± 0.17	0.016 ± 0.007	0.991 ± 0.0045

$\pi\{0\}$ is obtained from Eq. (A.11). The material coefficient D_A^{eff} has a lognormal distribution; therefore mean and standard deviation of $\ln(D_A^{\text{eff}})$ are reported. Taking the exponential of the reported mean value of $\ln(D_A^{\text{eff}})$ yields the median value of D_A^{eff} (in units of Pa).

the tensile and compressive regimes. Furthermore, we have confirmed the orthotropy of articular cartilage in both tension and compression. These results can be used to enhance theoretical models of articular cartilage, and provide greater insight into the structure–function relationships and physical environment of the chondrocytes in this tissue. The ability to capture the complex behavior of articular cartilage from one cubic sample of tissue using the technique described herein may also help in establishing standards for achieving a mechanically successful engineered replacement tissue.

Acknowledgements

This study was supported by grants from the National Institute of Arthritis and Musculoskeletal and Skin Diseases of the National Institutes of Health (AR 46532, AR43628 and AR46568).

Appendix. A

A theoretical analysis of the equilibrium response of cartilage is provided, using the framework of the triphasic theory of Lai et al. (1991), extended to account for a nonlinear strain-dependent response (Ateshian et al., 2003a, b). For simplicity, a one-dimensional analysis is performed which is strictly applicable to confined compression experiments (the full treatment of unconfined compression of an orthotropic triphasic material with tension–compression nonlinearity will be addressed in a future study). The purpose of this analysis is to demonstrate from theory that the experimental results of this study are consistent with the combined effects of tension–compression nonlinearity and osmotic swelling, and to explain how the free-swelling strain can be determined from the transition from a nonlinear to a linear regime in the stress–strain response.

Only equilibrium conditions are considered in the current analysis, in analogy to the experiments described above. In this case the total axial normal stress in cartilage, which is also the applied stress, is given by

$$\sigma = -\pi + \sigma^e, \tag{A.1}$$

where π is the osmotic pressure in the interstitial fluid and σ^e is the effective axial normal stress resulting from axial normal strain in the matrix. Let this solid matrix strain (the “true” strain relative to a reference configuration of zero strain) be given by E and let the (triphasic) aggregate modulus H_A be strain dependent under general conditions, so that a general constitutive relation for σ^e is given by $\sigma^e = H_A\{E\}E$. In addition, since the osmotic pressure is a function of proteoglycan fixed-charge density and since this fixed-charge density is

a function of the solid matrix strain (Lai et al., 1991), Eq. (A.1) can be rewritten as

$$\sigma\{E\} = -\pi\{E\} + H_A\{E\}E. \tag{A.2}$$

The dependence of π (and potentially H_A) on the ionic environment is implicit in this relation. When there is no applied stress on the tissue ($\sigma = 0$), the osmotic pressure π will place the tissue in an initial state of tensile free-swelling solid matrix strain E^0 given by the solution to the (generally nonlinear) equation

$$0 = -\pi\{E^0\} + H_A\{E^0\}E^0. \tag{A.3}$$

The experimental protocol of this study measures the applied strain E^a relative to this free-swelling configuration, where

$$E^a = E - E^0. \tag{A.4}$$

The applied strain is therefore equal to zero under free-swelling conditions when the “true” solid matrix strain is equal to E^0 . This distinction is important in the interpretation of results, which present σ versus E^a (Fig. 2). Eq. (A.2) can be differentiated with respect to E (or equivalently E^a since $dE = dE^a$) to yield the measured effective (biphase) modulus (the slope of the stress–strain curve)

$$H_A^{\text{eff}}\{E\} = \frac{d\sigma}{dE} = \frac{d\sigma}{dE^a} = \Pi\{E\} + H_A\{E\} + H'_A\{E\}E, \tag{A.5}$$

where $\Pi = -d\pi/dE = -d\pi/dE^a$, the rate of change of osmotic pressure with strain, is the contribution of fixed-charge density to the cartilage stiffness (Ateshian et al., 2003a). Based on the experimental results of Fig. 3, $H_A^{\text{eff}}\{E\}$ is nearly constant in the range of compressive solid matrix strains so that it is reasonable to assume

$$\Pi'\{E\} \approx H'_A\{E\} \approx 0 \text{ when } E < 0. \tag{A.6}$$

However, unlike $H_A\{E\}$ which depends on the collagen matrix and increases rapidly with tensile strain, Π depends only on fixed charge density and its strain-dependence in tension should be no different than in compression (under small strains). Based on Eq. (A.6), it can be concluded that Π is approximately constant for both tensile and compressive strains, in the range of small strains; equivalently, $\pi\{E\} \approx \pi\{0\} - \Pi E$ from a Taylor series expansion. Using this result into Eq. (A.2) yields

$$\sigma\{E\} \approx -\pi\{0\} + (\Pi + H_A\{E\})E. \tag{A.7}$$

This relationship implies that this study’s experiments can only yield $\Pi + H_A\{E\}$, but not Π or $H_A\{E\}$ on their own. In principle however, Π may be obtained from the knowledge of the fixed charge density as addressed in our upcoming study (Chahine et al., 2003, 2004).

Based on the experimental data of Figs. 2 and 3, the following constitutive relation is proposed:

$$\Pi + H_A \{E\} = \begin{cases} H_{-A}^{\text{eff}}, & E \leq 0, \\ H_{-A}^{\text{eff}} + D_A^{\text{eff}} E^{n-1}, & E \geq 0, \end{cases} \quad n \geq 2, \quad (\text{A.8})$$

or equivalently,

$$\sigma \{E\} \approx -\pi \{0\} + \begin{cases} H_{-A}^{\text{eff}} E, & E \leq 0, \\ H_{-A}^{\text{eff}} E + D_A^{\text{eff}} E^n, & E \geq 0, \end{cases} \quad n \geq 2, \quad (\text{A.9})$$

where H_{-A}^{eff} , D_A^{eff} and n are material coefficients independent of strain, H_{-A}^{eff} is the biphasic aggregate modulus in compression as measured in numerous studies. Alternatively, this relation can also be formulated in terms of $\sigma \{E^a\}$ versus E^a using Eq. (A.4),

$$\sigma \{E^a\} \approx \begin{cases} H_{-A}^{\text{eff}} E^a - D_A^{\text{eff}} (E^0)^n, & E^a \leq -E^0, \\ H_{-A}^{\text{eff}} E^a + D_A^{\text{eff}} [(E^a + E^0)^n - (E^0)^n], & E^a \geq -E^0, \end{cases} \quad n \geq 2, \quad (\text{A.10})$$

where it is recognized that since $\sigma = 0$ when $E^a = 0$ (no applied stress under free-swelling conditions),

$$\pi \{0\} = H_{-A}^{\text{eff}} E^0 + D_A^{\text{eff}} (E^0)^n. \quad (\text{A.11})$$

Clearly both Eqs. (A.9) and (A.10) are a representation of the same underlying phenomenon, namely that the modulus of cartilage remains constant under compressive matrix strains but rises rapidly with tensile matrix strains. Both equations are plotted in Fig. 8, with Fig. 8a ($\sigma \{E^a\}$ versus E^a) being representative of the experimental response shown in Fig. 2. Fig. 8b ($\sigma \{E\} + \pi \{0\} \approx \sigma^e \{E\}$ versus E) provides a more conventional representation of the tension–compression nonlinearity of the solid matrix, showing a linear response when the true matrix strain is compressive and a nonlinear response when the true matrix strain is tensile. Values of H_{-A}^{eff} , D_A^{eff} and n obtained from curvefitting the experimental stress–strain responses of this study are presented in Table 1.

Whether the tensile matrix strain results from osmotic swelling or from an applied tensile traction does not affect this one-dimensional analysis. The strain dependent modulus is given by the slope of the stress–strain response, or

$$\frac{d\sigma \{E^a\}}{dE^a} \approx \begin{cases} H_{-A}^{\text{eff}}, & E^a \leq -E^0, \\ H_{-A}^{\text{eff}} E^a + n D_A^{\text{eff}} (E^a + E^0)^{n-1} \equiv H_{+A}^{\text{eff}} \{E^a\}, & E^a \geq -E^0, \end{cases} \quad n \geq 2. \quad (\text{A.12})$$

This constitutive model *assumes* that the transition from compression to tension ($E = 0$ or equivalently $E^a = -E^0$) occurs at the point where a nonlinear response is observed and based on this assumption it is possible to identify the magnitude of the swelling

strain E^0 by increasing the applied compressive strain until the stress–strain response transitions from a nonlinear to a linear response. While it may seem paradoxical at first that the free-swelling strain is determined by compressing the tissue, Eqs. (A.10) and (A.12) clarify the rationale for this approach.

References

- Akizuki, S., Mow, V.C., Muller, F., Pita, J.C., Howell, D.S., Manicourt, D.H., 1986. Tensile properties of human knee joint cartilage: I. Influence of ionic conditions, weight bearing, and fibrillation on the tensile modulus. *Journal of Orthopaedic Research* 4, 379–392.
- Armstrong, C.G., Mow, V.C., 1982. Variations in the intrinsic mechanical properties of human articular cartilage with age, degeneration, and water content. *Journal of Bone and Joint Surgery-American Volume* 64, 88–94.
- Ateshian, G.A., Warden, W.H., Kim, J.J., Grelsamer, R.P., Mow, V.C., 1997. Finite deformation biphasic material properties of bovine articular cartilage from confined compression experiments. *Journal of Biomechanics* 30, 1157–1164.
- Ateshian, G.A., Chahine, N.O., Basalo, I.M., Hung, C.T., 2003a. The correspondence between equilibrium biphasic and triphasic material properties in mixture models of articular cartilage. *Journal of Biomechanics*, in press.
- Ateshian, G.A., Soltz, M.A., Mauck, R.L., Basalo, I.M., Hung, C.T., Lai, W.M., 2003b. The role of osmotic pressure and tension–compression nonlinearity in the frictional response of articular cartilage. *Transport in Porous Media* 50, 5–33.
- Basser, P.J., Schneiderman, R., Bank, R.A., Wachtel, E., Maroudas, A., 1998. Mechanical properties of the collagen network in human articular cartilage as measured by osmotic stress technique. *Archives of Biochemistry and Biophysics* 351, 207–219.
- Bursac, P., McGrath, C.V., Eisenberg, S.R., Stamenovic, D., 2000. A microstructural model of elastostatic properties of articular cartilage in confined compression. *Journal of Biomechanical Engineering* 122, 347–353.
- Bursac, P.M., Obitz, T.W., Eisenberg, S.R., Stamenovic, D., 1999. Confined and unconfined stress relaxation of cartilage: appropriateness of a transversely isotropic analysis. *Journal of Biomechanics* 32, 1125–1130.
- Chahine, N.O., Mantzaris, A.A., Chen, F.H., Hung, C.T., Ateshian, G.A., 2003. Direct measurement of osmotic pressure of glycosaminoglycan solutions by membrane osmometry. In: *Proceedings of the 2003 Summer Bioengineering Conference*, Key Biscayne, FL, Poster C22.
- Chahine, N.O., Chen, F.H., Hung, C.T., Ateshian, G.A., 2004. Direct measurement of the osmotic pressure of glycosaminoglycan solutions at room temperature in sodium chloride. In: *Proceedings of the 50th Annual Meeting of the Orthopaedic Research Society*, San Francisco, CA. Poster 524.
- Cohen, B., Lai, W.M., Mow, V.C., 1998. A transversely isotropic biphasic model for unconfined compression of growth plate and chondroepiphysis. *Journal of Biomechanical Engineering* 120, 491–496.
- Curnier, A., He, Q.C., Zysset, P., 1995. Conewise linear elastic materials. *Journal of Elasticity* 37, 1–38.
- Ehrlich, S., Wolff, N., Schneiderman, R., Maroudas, A., Parker, K.H., Winlove, C.P., 1998. The osmotic pressure of chondroitin sulfate solutions: experimental measurements and theoretical analysis. *Biorheology* 35, 383–397.

- Elliott, D.M., Narmoneva, D.A., Setton, L.A., 2002. Direct measurement of the poisson's ratio of human patella cartilage in tension. *Journal of Biomechanical Engineering* 124, 223–228.
- Farndale, R.W., Sayers, C.A., Barrett, A.J., 1982. A direct spectrophotometric microassay for sulfated glycosaminoglycans in cartilage cultures. *Connecting Tissue Research* 9, 247–248.
- Fortin, M., Soulhat, J., Shirazi-Adl, A., Hunziker, E.B., Buschmann, M.D., 2000. Unconfined compression of articular cartilage: nonlinear behavior and comparison with a fibril-reinforced biphasic model. *Journal of Biomechanical Engineering* 122, 189–195.
- Fry, H., Robertson, W.V., 1967. Interlocked stresses in cartilage. *Nature* 215, 53–54.
- Guilak, F., Ratcliffe, A., Mow, V.C., 1995. Chondrocyte deformation and local tissue strain in articular cartilage: a confocal microscopy study. *Journal of Orthopaedic Research* 13, 410–421.
- Huang, C.Y., Stankiewicz, A., Ateshian, G.A., Flatow, E.L., Bigliani, L.U., Mow, V.C., 1999. Anisotropy, inhomogeneity and tension–compression nonlinearity of human glenohumeral cartilage in finite deformation. *Transactions of the Orthopaedic Research Society* 24, 95.
- Huang, C.Y., Mow, V.C., Ateshian, G.A., 2001. The role of flow-independent viscoelasticity in the biphasic tensile and compressive responses of articular cartilage. *Journal of Biomechanical Engineering* 123, 410–417.
- Jurvelin, J.S., Buschmann, M.D., Hunziker, E.B., 1997. Optical and mechanical determination of poisson's ratio of adult bovine humeral articular cartilage. *Journal of Biomechanics* 30, 235–241.
- Kempson, G.E., Freeman, M.A., Swanson, S.A., 1968. Tensile properties of articular cartilage. *Nature* 220, 1127–1128.
- Kempson, G.E., Muir, H., Pollard, C., Tuke, M., 1973. The tensile properties of the cartilage of human femoral condyles related to the content of collagen and glycosaminoglycans. *Biochimica Biophysica Acta* 297, 456–472.
- Kwan, M.K., Lai, W.M., Mow, V.C., 1990. A finite deformation theory for cartilage and other soft hydrated connective tissues—I. Equilibrium results. *Journal of Biomechanics* 23, 145–155.
- Laasanen, M.S., Toyras, J., Korhonen, R.K., Rieppo, J., Saarakkala, S., Nieminen, M.T., Hirvonen, J., Jurvelin, J.S., 2003. Biomechanical properties of knee articular cartilage. *Biorheology* 40, 133–140.
- Lai, W.M., Hou, J.S., Mow, V.C., 1991. A triphasic theory for the swelling and deformation behaviors of articular cartilage. *Journal of Biomechanical Engineering* 113, 245–258.
- Lanir, Y., 1987. Biorheology and fluid flux in swelling tissues, II. Analysis of unconfined compressive response of transversely isotropic cartilage disc. *Biorheology* 24, 189–205.
- Maroudas, A., 1979. Physicochemical properties of articular cartilage. In: Freeman, M.A.R. (Ed.), *Adult Articular Cartilage*. Pitman Medical, Kent, pp. 215–290.
- Maroudas, A., Venn, M., 1977. Chemical composition and swelling of normal and osteoarthrotic femoral head cartilage. II. Swelling. *Annals of the Rheumatic Disease* 36, 399–406.
- Mow, V.C., Ratcliffe, A., 1997. Structure and function of articular cartilage and meniscus. In: Mow, V.C., Hayes, W.C. (Eds.), *Basic Orthopaedic Biomechanics*. Lippincott-Raven, Philadelphia, pp. 113–177.
- Mow, V.C., Kuei, S.C., Lai, W.M., Armstrong, C.G., 1980. Biphasic creep and stress relaxation of articular cartilage in compression? Theory and experiments. *Journal of Biomechanical Engineering* 102, 73–84.
- Myers, E.R., Lai, W.M., Mow, V.C., 1984. A continuum theory and an experiment for the ion-induced swelling behavior of articular cartilage. *Journal of Biomechanical Engineering* 106, 151–158.
- Narmoneva, D.A., Wang, J.Y., Setton, L.A., 1999. Nonuniform swelling-induced residual strains in articular cartilage. *Journal of Biomechanics* 32, 401–408.
- Roth, V., Mow, V.C., 1980. The intrinsic tensile behavior of the matrix of bovine articular cartilage and its variation with age. *Journal of Bone and Joint Surgery-American Volume* 62, 1102–1117.
- Schinagl, R.M., Gurskis, D., Chen, A.C., Sah, R.L., 1997. Depth-dependent confined compression modulus of full-thickness bovine articular cartilage. *Journal of Orthopaedic Research* 15, 499–506.
- Schmidt, M.B., Mow, V.C., Chun, L.E., Eyre, D.R., 1990. Effects of proteoglycan extraction on the tensile behavior of articular cartilage. *Journal of Orthopaedic Research* 8, 353–363.
- Schwartz, M.H., Leo, P.H., Lewis, J.L., 1994. A microstructural model for the elastic response of articular cartilage. *Journal of Biomechanics* 27, 865–873.
- Setton, L.A., Tohyama, H., Mow, V.C., 1998. Swelling and curling behaviors of articular cartilage. *Journal of Biomechanical Engineering* 120, 355–361.
- Soltz, M.A., Ateshian, G.A., 2000. A conewise linear elasticity mixture model for the analysis of tension–compression nonlinearity in articular cartilage. *Journal of Biomechanical Engineering* 122, 576–586.
- Soulhat, J., Buschmann, M.D., Shirazi-Adl, A., 1999. A fibril-network-reinforced biphasic model of cartilage in unconfined compression. *Journal of Biomechanical Engineering* 121, 340–347.
- Urban, J.P., Maroudas, A., Bayliss, M.T., Dillon, J., 1979. Swelling pressures of proteoglycans at the concentrations found in cartilaginous tissues. *Biorheology* 16, 447–464.
- Wang, C.C., Deng, J.M., Ateshian, G.A., Hung, C.T., 2002. An automated approach for direct measurement of two-dimensional strain distributions within articular cartilage under unconfined compression. *Journal of Biomechanical Engineering* 124, 557–567.
- Wang, C.C.B., Chahine, N.O., Hung, C.T., Ateshian, G.A., 2003. Optical determination of anisotropic properties of bovine articular cartilage in compression. *Journal of Biomechanics* 36, 339–353.
- Wong, M., Ponticello, M., Kovanen, V., Jurvelin, J.S., 2000. Volumetric changes of articular cartilage during stress relaxation in unconfined compression. *Journal of Biomechanics* 33, 1049–1054.
- Woo, S.L., Akeson, W.H., Jemmott, G.F., 1976. Measurements of nonhomogeneous, directional mechanical properties of articular cartilage in tension. *Journal of Biomechanics* 9, 785–791.
- Woo, S.L., Lubock, P., Gomez, M.A., Jemmott, G.F., Kuei, S.C., Akeson, W.H., 1979. Large deformation nonhomogeneous and directional properties of articular cartilage in uniaxial tension. *Journal of Biomechanics* 12, 437–446.